# Laser self-mixing interferometry for direct displacement reconstruction using deep learning

**Qinyu Li[1], Li Quan[1], Wei Xia, and Dongmei Guo***

School of Computer and Electronic Information, Nanjing Normal University, Nanjing 210023, China

* Corresponding author: guodongmei@njnu.edu.cn
[1] These authors contributed to the work equally and should be regarded as co-first authors

**Abstract:**
In this paper, we propose a displacement reconstruction method based on laser self-mixing interferometer using deep learning. A novel Direct Displacement Reconstruction Network (DDR-Net) has been designed to demodulate the self-mixing interference (SMI) signals. The DDR-Net takes the original SMI signal as the input, using the target displacement as the training label to achieve an end-to-end regression task. Experimental results demonstrate that DDR-Net effectively reconstructs target displacement using training data collected from real experimental environments, showcasing robust generalization across different displacement modes and noisy conditions. Multiple random experiments reveal that the relative measurement error of the reconstructed displacement consistently remains below 1%. This method significantly simplifies the data processing workflow, highlighting its potential for applications in laser self-mixing sensing and offering new insights for tackling complex measurement tasks.

## 1. Introduction：

Self-mixing interference (SMI), also known as optical feedback interference (OFI), occurs when a small portion of light emitted from a laser is reflected or backscattered by an external object. The reflected light then reenters the laser cavity, resulting in modulation of both the amplitude and frequency of the laser field [1-2]. It is a promising technique for displacement sensing [3-5], vibration [6-7], velocity [8-9], angle [10-11], and other parameters [12-13] due to its inherent simplicity, compactness, robustness, and self-aligning capabilities. Displacement sensing is a primary application of SMI. At its most basic level, a measurement resolution of half-wavelength can be achieved by counting the peaks of the interference signal. To further enhance the displacement measurement resolutions, numerous signal processing algorithms have been proposed, based on fringe detection methods or phase demodulation techniques [14-17].

In recent years, deep learning has made significant advancements in fields such as

image recognition, time series forecasting, and natural language processing. The application of deep learning in SMI signal analysis has also attracted the attention of many researchers. For instance, Ahmed et al. developed a generative adversarial network (GAN)-based framework to denoise SMI signals across different noise conditions, achieving high signal-to-noise ratio (SNR) improvements under different optical feedback levels [18]. Barland et al. proposed a convolutional neural network (CNN) method for displacement sensing, enabling high-precision displacement reconstruction of noisy SMI signals. By incorporating the velocity of the SMI signal as an input feature, this approach effectively mitigates distortions caused by hardware and ensures robust performance across different signal shapes and alignment conditions [19]. After that, Matha et al. advanced a multi-channel CNN architecture tailored for the displacement measurement of single target based on SMI principle. The input utilizes a three-channel structure, where each channel corresponds to a distinct SMI signal. This configuration ensures the model remains accurate and robust, even in the presence of two channel degradation [20].

In this paper, we design a novel Direct Displacement Reconstruction Network (DDR-Net) to reconstruct the target displacement from SMI signals. The DDR-Net takes the original SMI signal as the input, using the target displacement as the training label, exhibiting good generalization abilities across various displacement modes and noisy conditions. The network has been trained on data from the real experimental environments. The principles of SMI-based displacement measurement and the methods of deep learning are introduced in detail below. Furthermore, extensive random experimental results validate the feasibility and prediction accuracy of DDR-Net, while noise performance analysis confirms its robustness.

## 2. Methodology

### 2.1 SMI-based displacement sensing principle

The typical SMI theoretical framework can be simplified as an interference effect in an equivalent Fabry–Perot cavity. The output power $P_t$ can be expressed as:

$$P_t = P_0[1 + m\cos(\varphi_t)], \tag{1}$$

where $P_0$ is the output without SMI, $m$ represents the modulation index, which is impacted by the reflection coefficient of the target surface, and $\varphi_t$ denotes the phase in the presence of SMI. Note that $\varphi_t$ can be calculated by the well-known excess phase equation with the original phase $\varphi_0$ as:

$$\varphi_0 = \varphi_t + C\sin(\varphi_t - \arctan\alpha), \tag{2}$$

where $C$ and $\alpha$ represent the optical feedback factor and the linewidth enhancement factor, respectively. The relationship between phase and displacement can be derived

from Eq. (3) and Eq. (4):

$$\varphi_0 = \frac{4\pi L_0}{\lambda_0}, \tag{3}$$

$$\Delta\varphi_t = \frac{4\pi\Delta L_t}{\lambda}, \tag{4}$$

where $\lambda$ and $\lambda_0$ denote the wavelengths with and without SMI effect, respectively. $L_t$ is the external cavity length, and $L_0$ is the initial value. The displacement $x$ of the target object can be derived from $\Delta\varphi_t$ based on Eq. (5):

$$x = \Delta L_t = \Delta\varphi_t \cdot \frac{\lambda}{4\pi}. \tag{5}$$

Based on this, under known wavelength and weak feedback conditions, a linear mapping relationship exists between the unique phase solution $\varphi_t$ and the target displacement $x$. Compared to previous methods, such as phase unwrapping techniques or modulation methods applied to SMI signals, the deep learning approach is more straightforward. For instance, Chen et al. based on the concept of transfer learning, utilized simulated data to train a model for phase extraction from SMI signals, which was subsequently converted into displacement [21]. However, this approach introduced linear errors based on Eq. (5). To solve this problem, by constructing a customized neural network model and leveraging its powerful nonlinear mapping ability and automatic feature extraction capabilities, it becomes possible to directly reconstruct the target displacement from the SMI signals.

## 2.2 Dataset

The SMI signals have been collected from a self-mixing interference experimental setup, as shown in Fig. 1. The system mainly consists of the following components: a laser diode (LD, 650nm, 20mW), a current source (Thorlabs, LCD201C) and a temperature-controlled source (Thorlabs, TED200C) for LD, a nano-displacement stage (PI, P621.2CD), and silicon target. In the experiments, the output power of the transmitted light can be controlled by adjusting the neutral density filter (ND) to obtain SMI signals under weak feedback conditions. The piezoelectric transducer (PZT) is capable of producing deformation with nanometer precision under the control of the input voltage, which is used to simulate the micro-displacement of the target. The beam from the semiconductor laser is incident on the surface of the silicon wafer through a ND, and the reflected light carries the target motion information back to the laser cavity, where a self-mixing interference effect occurs with the intra-cavity light. Ultimately, the SMI signal is received by a photodetector integrated at the back end of the semiconductor laser and transmitted to a PC for signal processing and display after acquisition by an oscilloscope.

The normalized SMI signals are fed into the constructed model, enabling the extraction of the motion information of the target. Once the network architecture is

determined, it must be trained using known data. It is widely recognized that the representational capacity of a neural network relies on an adequate number of layers and units, coupled with a diverse dataset rich in features. Consequently, given sufficient computational resources and training duration, a well-optimized network can effectively fit the training data, yielding improved performance. Nonetheless, a primary challenge in SMI measurements stems from fluctuations in alignment conditions across individual measurements. Specifically, the speckle patterns generated by the reflected light from a scattering target result in variations in the feedback intensity parameter throughout the measurement process. As a result, the trained network requires robust generalization capabilities to accurately identify features in unseen data.

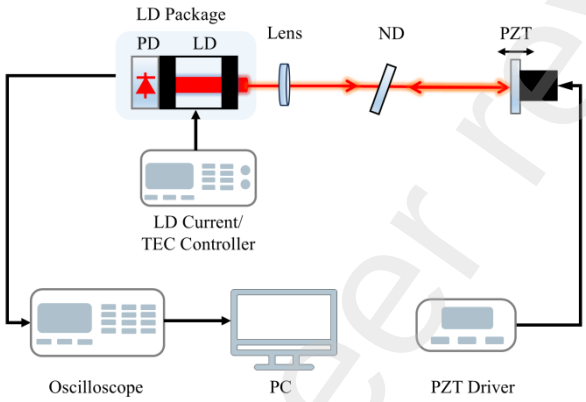


**Fig. 1.** Experimental system block diagram.

To evaluate the network's displacement reconstruction performance, an experimental dataset was collected under diverse conditions, including varying displacement modes and different beam-target alignment conditions. The training data consists solely of experimental measurements of SMI signals generated by a target under periodic displacements. Specifically, seven frequency points were evenly selected within the range of 10 Hz to 22 Hz, with each frequency corresponding to five different displacement amplitudes ranging from 2μm to 4μm. Additionally, multiple sets of SMI signals were obtained by fine-tuning the tilt angle of the laser support structure to simulate varying alignment conditions. The experiment adopted a sampling frequency of 10 kHz, collecting 22 datasets under each condition. To facilitate network processing, a windowing function was applied to each sample, segmenting it into 150ms data fragments. In total, the network input comprised approximately 60,270 data fragments, each 150ms long, with 20% of the samples reserved for the validation set. To enhance the generalization capability of the model, the order of the samples was randomized in each training epoch.

## 2.3 The DDR-Net Framework

To accurately reconstruct the target displacement and rebuild the target motion trajectory based on the SMI signal, we have transformed this task into a "regression"

problem in deep learning. Based on the classic convolutional neural network (CNN) structure and the long short-term memory (LSTM) structure, we developed a hybrid model, called the Direct Displacement Reconstruction Neural Network (DDR-Net). The CNN is a deep learning architecture that excels at capturing local dependencies and patterns in time-series or spatial data through the application of convolutional kernels with weight-sharing mechanisms [22-23]. The LSTM is a recurrent neural network variant designed to effectively model long-term dependencies in sequential data by mitigating the vanishing gradient problem through its memory cell and gating mechanisms [24]. By integrating the strengths of CNN in extracting local features and the capability of LSTM in modeling sequential dependencies, DDR-Net enhance the precision and robustness of displacement reconstruction from SMI signals.

As shown in Fig. 2, the model consists of three parts: (1) CNN part: it contains three convolutional layers with the number of convolutional kernels of 32, 64, and 128, respectively, and the size of the convolutional kernel is 3 × 1 with the step size of 1. Each convolutional layer is followed by a maximal pooling layer with the size of the pooling kernel of 2 × 1, which is used to gradually extract the local features of the SMI signals and to reduce the dimensionality of the data. (2) LSTM part: a two-layer bi-directional LSTM structure, each layer contains 128 hidden units, which is able to capture the long-term dependencies in the signal and enhance the modeling ability of the backward and forward correlation of time series. (3) Fully connected layer: consists of two linear transformation layers and ReLU activation function, which maps the high-dimensional features of the LSTM output to the target displacement sequence, and the final output shape is (1, 1500). Therefore, DDR-Net employs an end-to-end training approach to effectively eliminate the complex signal processing steps required by traditional methods.

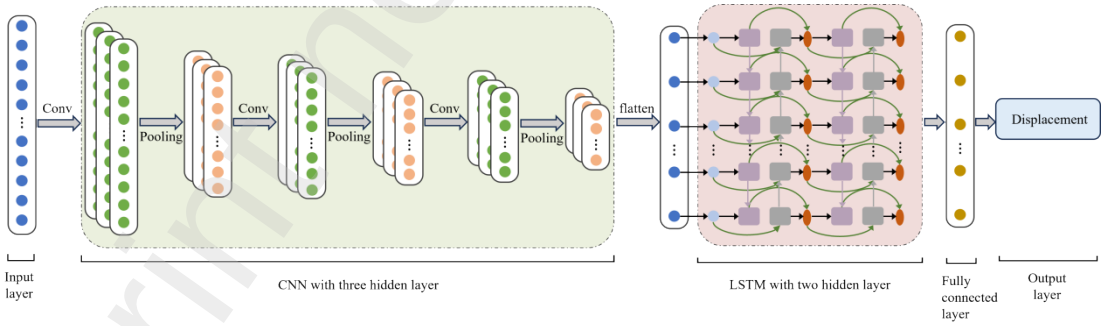


**Fig. 2.** Schematic diagram of the DDR-Net.

## 2.4 Loss function and evaluation index

During model training, the mean squared error (MSE) Loss function is adopted due to its effectiveness and wide application in regression tasks. MSE is particularly suitable for this scenario, as its squared error term emphasizes large deviations between predictions and ground truth, thereby encouraging the network to minimize substantial errors and improve overall prediction accuracy. Notably, in regression tasks, the

derivative of MSE Loss becomes zero when the predicted value matches the true value, which facilitates effective gradient-based updates. The MSE Loss is defined as Eq. (6):

$$\mathrm{MSE} = \frac{1}{N}\sum_{i=1}^{N}(x_i - \hat{x}_i)^2, \tag{6}$$

where N represents the number of samples, $x_i$ denotes the true displacement value, and $\hat{x}_i$ is the predicted displacement value. The model parameters are optimized by minimizing MSE Loss, so that the predicted displacement values are as close as possible to the true values.

Additionally, the coefficient of determination ($R^2$) is introduced to evaluate the model's ability to explain the variance in the target data. As a complementary metric to MSE, $R^2$ quantifies how well the predicted values account for the observed variability. The value of $R^2$ ranges from 0 to 1, where $R^2 = 1$ indicates a perfect prediction and $R^2 = 0$ suggests that the model fails to explain any variance in the data. The closer the $R^2$ is to 1, the stronger the explanatory power of the model, and the better its performance. Since the proposed model contains only a single predictor variable, it avoids the potential overestimation of $R^2$ values that can arise in multivariable models due to an excess of predictor variables. The coefficient of determination $R^2$ is calculated as Eq. (7):

$$R^2 = 1 - \frac{SS_{res}}{SS_{tot}}, \tag{7}$$

where $SS_{res}$ is the sum of squares of residuals, also known as the sum of squared errors, computed as $SS_{res} = \sum_{i=1}^{N}(x_i - \hat{x}_i)^2$ and $SS_{tot}$ is the total sum of squares, given by $SS_{tot} = \sum_{i=1}^{N}(x_i - \bar{x})^2$, and $\bar{x}$ represents the mean of the actual values. By considering both of these metrics, we can comprehensively evaluate the performance of the model.

## 2.5 Network Training Details

The training process of the model is illustrated in Fig. 3. Both the training and validation loss curves exhibit an overall downward trend, initially decreasing rapidly before gradually stabilizing. At the end of the training, the $R^2$ coefficients of determination for the training sets approach 1, indicating that the model effectively fits the data during the training phase. These observations from the training process suggest that the model successfully captures the underlying trends in the data and demonstrates strong generalization capabilities. Additionally, an early stopping mechanism was employed to prevent overfitting, where the optimal model parameters were saved if the validation loss failed to improve over 10 consecutive epochs.

The initial learning rate was set at $10^{-3}$, and the training process spanned 100 epochs. To optimize training efficiency, the Adam algorithm was employed, capitalizing on its adaptive learning rate capabilities. Furthermore, a learning rate decay strategy,

ReduceLROnPlateau, was implemented to enhance performance. Under this approach, the learning rate was reduced by 10% whenever the validation loss failed to decrease over five consecutive epochs. This approach significantly improved convergence stability. The neural network training was conducted on a system equipped with an NVIDIA GeForce RTX 4060 GPU, an Intel i5-13600KF CPU and Python 3.7. The displacement reconstruction of an SMI signal over a 150 ms duration was achieved with a computation time of only 5.2 ms, demonstrating the model's high processing efficiency.

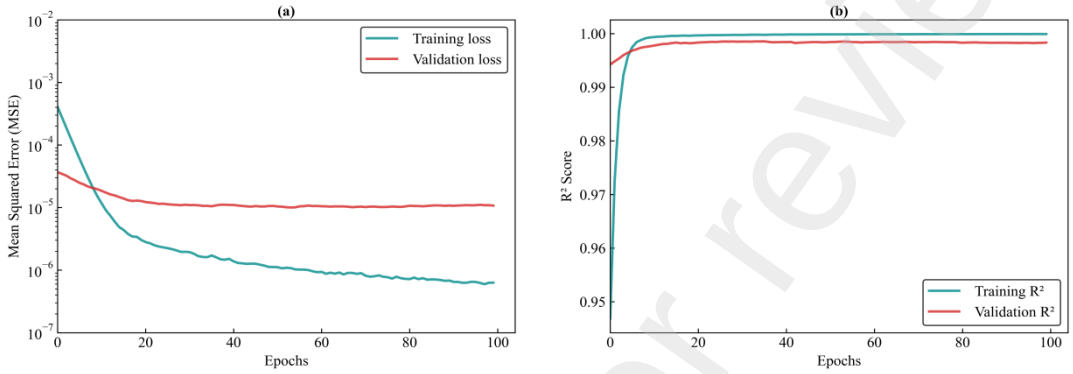


**Fig. 3.** Model training process. (a) MSE Loss curve. (b) $R^2$ curve.

## 3. Results

### 3.1 Feasibility and accuracy

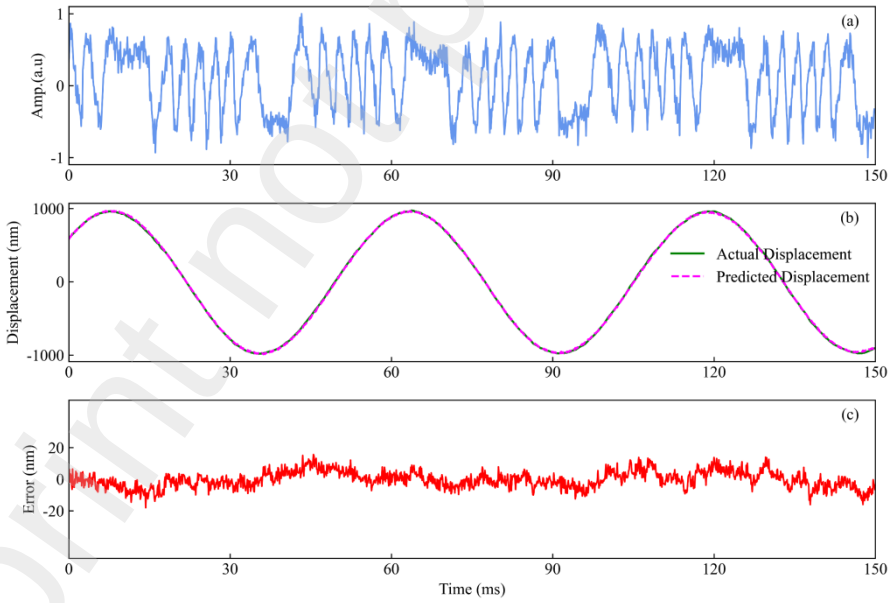


**Fig. 4.** Displacement reconstruction results of the first experimental test dataset: (a) SMI signal. (b) Displacement reconstruction results of DDR-Net. (c) Displacement reconstruction error.

During training, the model effectively learned the nonlinear mapping between SMI signals and target displacement. After training, an independent test dataset, distinct from the training dataset, was employed to assess the model's displacement

reconstruction performance. Given that SMI signals acquired in real experimental environments are susceptible to noise and other disturbances, a repeatability test was conducted using a batch of SMI signals obtained under identical experimental parameters to ensure the reliability of the results. The displacement reconstruction results from the first test dataset are presented in Fig. 4. Fig. 4(a) displays the input SMI signal with a target motion frequency of 18 Hz and a peak-to-peak amplitude of 2μm, while Figs. 4(b) and 4(c) depict the reconstructed displacement and the corresponding reconstruction error, respectively, demonstrating its excellent performance in displacement reconstruction. To further assess the model's stability, ten repeated tests were conducted on the representative signal sample shown in Fig. 4(a), with the results summarized in Table I. The data in Table I reveal that the DDR-Net maintains consistent performance across the ten tests, with the maximum reconstruction error ranging from 12 to 18 nm, confirming its robustness and precision accuracy in practical applications.

**Table I** Results of ten repeated tests from the first set

| Group | Target(nm) | Reconstruction (nm) | Maximum error (nm) |
|---|---|---|---|
| 1 | 1997 | 1984 | 13 |
| 2 | 2003 | 2017 | 14 |
| 3 | 1992 | 1980 | 12 |
| 4 | 2000 | 2016 | 16 |
| 5 | 1995 | 1983 | 12 |
| 6 | 2002 | 1987 | 15 |
| 7 | 2007 | 2019 | 12 |
| 8 | 1994 | 2012 | 18 |
| 9 | 1998 | 2014 | 16 |
| 10 | 2001 | 1989 | 12 |

The displacement reconstruction results of the second experimental test dataset are shown in Fig. 5. Fig. 5(a) presents the input SMI signal, characterized by a target motion frequency of 20 Hz and a peak-to-peak displacement of 3.5 μm. Fig. 5(b) illustrates the displacement reconstruction results of the DDR-Net, while Fig. 5(c) illustrates the corresponding reconstruction error. Compared to the first experimental dataset, the reconstruction error increases in this case, attributable to the higher frequency and amplitude, which result in more fringes within the same time segment. This suggests that as the complexity of the SMI signal increases, the model's performance degrades relative to simpler case.

To comprehensively evaluate the generalization capability of DDR-Net, an analysis

was performed using 250 experimental sets. Fig.6 (a) presents the reconstruction error distribution at a fixed frequency of 17 Hz for displacement amplitudes of 2 μm, 2.5 μm, 3 μm, and 4 μm. The experimental results indicate that, while the relative error of the reconstructed peak-to-peak displacement increases slightly with amplitude, it still remains low, with a maximum relative error below 1%. This demonstrates the high stability and accuracy of the model in displacement reconstruction. Furthermore, Fig. 6 (b) illustrates the reconstruction error under a fixed displacement amplitude of 3.5 μm across frequencies ranging from 11 Hz to 19 Hz. Although the reconstruction error exhibits some fluctuations, the variation remains minor, and the overall error remains within an acceptable range. This indicates that DDR-Net can effectively adapt to displacement reconstruction tasks across different frequency conditions. Based on all these experimental results, it can be concluded that DDR-Net demonstrates robust displacement reconstruction performance under different displacement amplitudes and frequency conditions, confirming its strong adaptability and robustness.

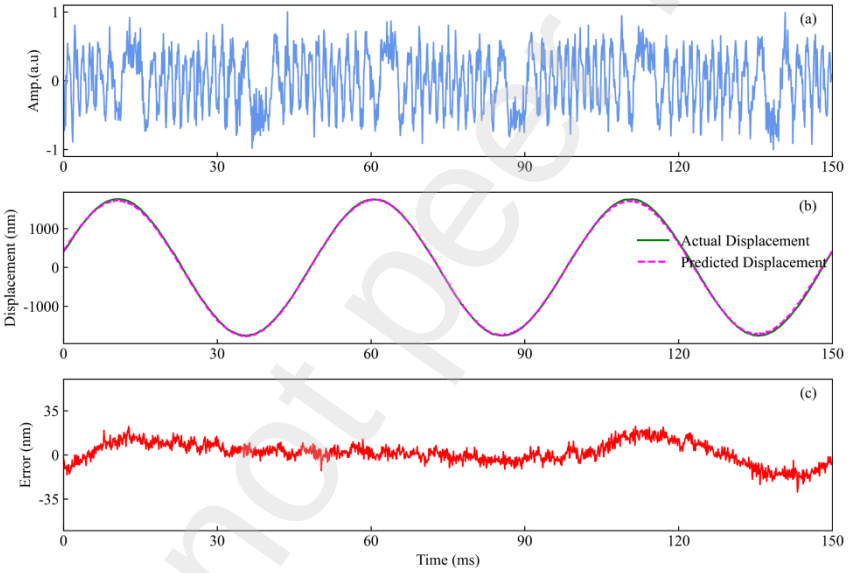


**Fig. 5.** Displacement reconstruction results of the second experimental test dataset: (a) SMI signal. (b) Displacement reconstruction results of DDR-Net. (c) Displacement reconstruction error.

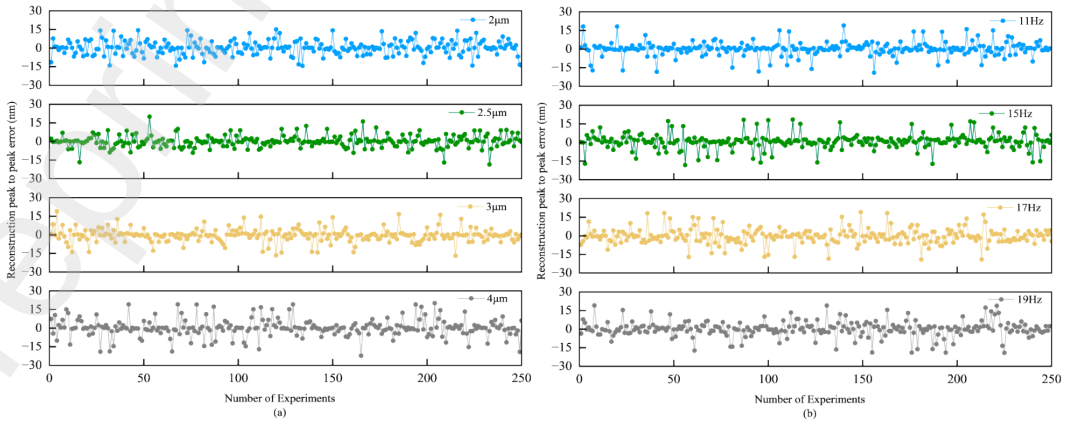


**Fig. 6.** Distribution of displacement reconstruction errors of the DDR-Net under

different experimental conditions:(a) 2 μm, 2.5 μm, 3 μm, and 4 μm displacement amplitudes at the fixed frequency of 17 Hz. (b) 11 Hz to 19 Hz under the fixed 3.5 μm displacement amplitude.

## 3.2 Anti-noise performance analysis

Due to the inherently low noise level of the experimental system, the noise robustness of DDR-Net was evaluated by artificially adding Gaussian white noise of varying intensities to 1,000 experimental sets. This yielded a test dataset with signal-to-noise ratios (SNRs) ranging from -2 dB to 20 dB. By introducing noise at different SNR levels, the interference conditions in real-world applications can be more accurately simulated. The resulting performance of DDR-Net under different noise conditions is presented in Fig. 7.

To evaluate the model's performance quantitatively, the coefficient of determination ($R^2$) was used as the evaluation metric. As depicted in Fig. 7, the $R^2$ score of the DDR-Net increases markedly with SNR rising from -2 dB to 20 dB, improving from approximately 0.62 to about 0.99. In the low SNR region (-2 dB to 4 dB), the curve exhibits a sharp upward trend, indicating that the performance is highly sensitive to improvements in SNR. Notably, even under the challenging -2 dB condition, the $R^2$ score still reaches 0.62. In the high SNR region (above 12 dB), the curve levels off, approaching saturation, with the $R^2$ score nearing 1.0. This demonstrates the model's robust noise resistance capability.

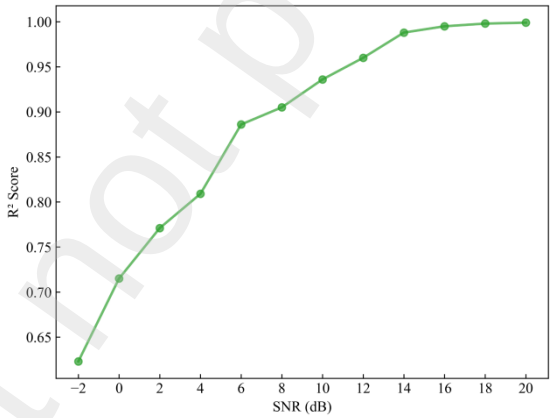


**Fig. 7.** Analysis of the anti-noise performance of displacement reconstruction for DDR-Net.

## 4. Conclusion

In contrast to many previous studies that build datasets from simulated data, all of our datasets are sourced from real experiments. Inevitably, various sources of errors exist in the experimental data, which affect the signal processing and the accuracy of the results. These errors may originate from multiple factors, such as interference in the optical path, nonlinear responses of the instruments and environmental conditions. Furthermore, there may be errors in the actual motion of the PZT. Due to the imperfections in the driving signal generator and the mechanical characteristics of the

system, the actual motion trajectory of the PZT may deviate from the theoretical sine wave. This deviation directly impacts the actual displacement data used as the training label, thereby influencing the accuracy and evaluation results during the model training process.

The interactions of these sources of error contribute to a certain degree of deviation between the final reconstruction results of the model and the actual displacement. Despite the inevitable presence of noise and errors, experimental results demonstrate that the model exhibits high robustness in both the training data collection environment and test data collection environment, consistently reconstructing the target displacement. From another perspective, this not only validates the resilience of the model to noise and error environments but also provides direction for subsequent optimization efforts on how to better handle experimental errors. Future work will focus on optimizing error suppression strategies during both data preprocessing and model training, such as using multi-sensor fusion methods to reduce label biases caused by PZT motion errors. Moreover, combining dynamic adjustments of experimental conditions and adversarial training approaches is expected to further enhance the adaptability and stability of the model across various experimental settings.

In conclusion, we develop a simple and efficient DDR-Net model for directly reconstructing target displacement from the SMI signal. All training and test data are derived from real experimental setups, ensuring robust generalization and reliability, which translates into high accuracy in practical applications. The hybrid model takes the real SMI signal as input, with the actual target displacement used as the training label. Experimental results demonstrate that DDR-Net can accurately predict the target displacement, with a maximum relative error below 1%. Notably, in complex signal processing and large-scale data analysis, neural networks exhibit distinct advantages. They can extract key information from complex signals and efficiently process large-scale data, providing an ideal solution to address the limitations of traditional SMI measurement techniques.

**Funding.** This work was funded by the National Natural Science Foundation of China (51875292).

## Reference:

[1] A. Jha, L. R. Cenkeramaddi, and S. Royo, "Generalized multi-cavity laser self-mixing interferometry based on scattering theory," Opt. Express 31, 16508–16522 (2023). https://doi.org/10.1364/OE.484086.

[2] T. Taimre, M. Nikolic, K. Bertling, Y. Lim, T. Bosch, and A.D. Rakić, "Laser feedback interferometry: a tutorial on the self-mixing effect for coherent sensing," Adv. Opt. Photonics 7,

570-631 (2015). https://doi.org/10.1364/AOP.7.000570.
[3] D. Guo, L. Shi, Y. Yu, W. Xia, and M. Wang, "Micro-displacement reconstruction using a laser self-mixing grating interferometer with multiple-diffraction," Opt. Express 25, 31394-31406 (2017). https://doi.org/10.1364/OE.25.031394.
[4] A. Albert, S. Donati, and S.-L. Lee, "Self-mixing interferometry on long distance: theory and experimental validation," IEEE Trans. Instrum. Meas. 73, 1–8 (2024). https://doi.org/10.1109/TIM.2024.3485399.
[5] M. Norgia, D. Melchionni and A. Pesatori, "Self-mixing instrument for simultaneous distance and speed measurement," Opt. Lasers Eng. 99, 31–38 (2017). https://doi.org/10.1016/j.optlaseng.2016.10.013.
[6] M. Usman, U. Zabit, O.D. Bernal, G. Raja and T. Bosch, "Detection of multimodal fringes for self-mixing-based vibration measurement," IEEE Trans. Instrum. Meas. 69, 258–267 (2020). https://doi.org/10.1109/TIM.2019.2895928.
[7] K. Otsuka, K. Abe, J.-Y. Ko, and T.-S. Lim, "Real-time nanometer-vibration measurement with a self-mixing microchip solid-state laser," Opt. Lett. 27, 1339–1341 (2002). https://doi.org/10.1364/OL.27.001339.
[8] L. Scalise, Y. Yu, G. Giuliani, G. Plantier and T. Bosch, "Self-mixing laser diode velocimetry: application to vibration and velocity measurement," IEEE Trans. Instrum. Meas. 53, 223–232 (2004). https://doi.org/10.1109/TIM.2003.822194.
[9] L. Rovati, S. Cattini and N. Palanisamy, "Measurement of the fluid-velocity profile using a self-mixing superluminescent diode," Meas. Sci. Technol. 22, 025402 (2011). https://doi.org/10.1088/0957-0233/22/2/025402.
[10] S. Donati, D. Rossi, and M. Norgia, "Single channel self-mixing interferometer measures simultaneously displacement and tilt and yaw angles of a reflective target," IEEE J. Quantum Electron. 51, 1–8 (2015). https://doi.org/10.1109/JQE.2015.2497237.
[11] B. Yang, D. Wang, L. Zhou, S. Wu, R. Xiang, W. Zhang, H. Gui, J. Liu, H. Wang, L. Lu, and B. Yu, "A ultra-small-angle self-mixing sensor system with high detection resolution and wide measurement range," Opt. Laser Technol. 91, 92-97 (2017). https://doi.org/10.1016/j.optlastec.2016.11.024.
[12] A. A. A. Bakar, Y. L. Lim, S. J. Wilson, M. Fuentes, K. Bertling, T. Taimre, T. Bosch and A. D. Rakić, "On the feasibility of self-mixing interferometer sensing for detection of the surface electrocardiographic signal using a customized electro-optic phase modulator," Physiol. Meas. 34, 281–289 (2013). https://doi.org/10.1088/0967-3334/34/2/281.
[13] S. Maqueda, J. Perchoux, C. Tronche, J. J. I. González, M. Genetier, M. Lavayssière, and Y. Barbarin, "Demonstration of pressure wave observation by acousto-optic sensing using a self-mixing interferometer," Sensors 23, 3720 (2023). https://doi.org/10.3390/s23073720.
[14] V. Contreras, J. Toivonen, and H. Martinez, "Enhanced self-mixing interferometry based on volume Bragg gratings and laser diodes emitting at 405-nm wavelengths," Opt. Lett. 42, 2141-2144 (2017). https://doi.org/10.1364/OL.42.002221.
[15] S. Amin, "Implementation of Hilbert transform based high-resolution phase unwrapping method for displacement retrieval using laser self-mixing interferometry sensor," Opt. Laser Technol. 149, 107887 (2022). https://doi.org/10.1016/j.optlastec.2022.107887.
[16] K. Kou, X. Li, L. Li, H. Li, and T. Wu, "Absolute distance estimation with improved genetic algorithm in laser self-mixing scheme," Opt. Laser Technol. 68, 113–119 (2015). https://doi.org/10.1016/j.optlastec.2014.11.016.
[17] O. D. Bernal, H. C. Seat, U. Zabit, F. Surre, and T. Bosch, "Robust detection of non-regular interferometric fringes from a self-mixing displacement sensor using bi-wavelet transform," IEEE Sens. J. 16, 7903–7910 (2016). https://doi.org/10.1109/JSEN.2016.2599702.
[18] I. Ahmed, U. Zabit, and A. Salman, "Self-mixing interferometric signal enhancement using generative adversarial network for laser metric sensing applications," IEEE Access 7, 174641-174650 (2019). https://doi.org/10.1109/ACCESS.2019.2957272.
[19] S. Barland, and F. Gustave, "Convolutional neural network for self-mixing interferometric displacement sensing," Opt. Express 29, 11433-11444 (2021). https://doi.org/10.1364/OE.419844.
[20] R. Matha, S. Barland, and F. Gustave, "High-availability displacement sensing with multi-channel self-mixing interferometry," Opt. Express 31, 21458-21467 (2023). https://doi.org/10.1364/OE.485955.
[21] J. Chen, X. Wang, Y. Wu, Y. Yang, M. Qiu, M. Wang, and Y. Li, "Self-mixing interferometry

based on a phase decomposition neural network," Opt. Eng. 61, 054103 (2022). https://doi.org/10.1117/1.OE.61.5.054103.
[22] A. Krizhevsky, I. Sutskever, and G. E. Hinton, "ImageNet classification with deep convolutional neural networks," Commun. ACM 60, 84-90 (2017). https://doi.org/10.1145/3065386.
[23] K. He, X. Zhang, S. Ren, and J. Sun, "Deep residual learning for image recognition," Proc. IEEE Conf. Comput. Vis. Pattern Recognit., 770-778 (2016). https://doi.org/10.1109/CVPR.2016.90.
[24] S. Hochreiter and J. Schmidhuber, "Long short-term memory," Neural Comput. 9, 1735-1780 (1997). https://doi.org/10.1162/neco.1997.9.8.1735.